Intermetallics xxx (2009) 1–6

Contents lists available at ScienceDirect

Intermetallics

journal homepage: www.elsevier.com/locate/intermet

Microstructure-hardness relationship of Al–($L1_2$)Al_3Ti nanocomposites prepared by rapid solidification processing

S.S. Nayak [a,*], S.K. Pabi [a], D.H. Kim [b], B.S. Murty [c]

[a] Department of Metallurgical and Materials Engineering, Indian Institute of Technology, Kharagpur 721 302, India
[b] Center for Nanocrystalline Materials, Department of Metallurgical Engineering, Yonsei University, Seoul 120-749, South Korea
[c] Department of Metallurgical and Materials Engineering, Indian Institute of Technology Madras, Chennai 600 036, India

ARTICLE INFO

Article history:
Received 25 June 2009
Received in revised form
14 September 2009
Accepted 15 September 2009
Available online xxx

Keywords:
A. Composites
A. Trialuminides
B. Precipitates
C. Rapid solidification processing
B. Mechanical properties at ambient temperature
A. Nanostructured intermetallics

ABSTRACT

We report here successful synthesis of Al-based nanocomposites with $L1_2$–Al_3Ti particles in binary Al–Ti (4.1, 5, 8.3, 10, 15 and 20% Ti) and ternary Al-1.6Ti-0.5Cr, Al-3.2Ti-1.0Cr and Al-6.3Ti-2.0Cr alloys, by rapid solidification processing. The microstructure of all the alloys consists of uniform distribution of nanocrystalline $L1_2$–Al_3Ti intermetallic in ultra-fine α-Al matrix. The volume fraction of $L1_2$–Al_3Ti phase in the as-spun ribbons was found to increase with the Ti content in the binary alloys with exception of Al-20% Ti alloy, which formed equilibrium DO_{22}–Al_3Ti. The α-Al grains were measured to be in the size range 0.5–1.0 μm embedded with $L1_2$–Al_3Ti particles of ~50 nm diameter. Nanoindentation as well as microhardness of nanocomposites in binary Al–Ti alloys measure hardness value of 3.75 GPa (367 VHN). The nanocomposites formed by rapid solidification processing retain about 70–85% of its room temperature hardness even at 500 °C for 100 h, while the hardness of conventional Al alloys such as 2017 is almost lost at 350 °C in 30 min.

1. Introduction

High temperature strength of Al alloys is improved by adding transition metals those form intermetallic phases with Al [1]. Aluminum alloys reinforced with aluminide particles ($NiAl_3$, $FeAl_3$, $TiAl_3$, etc.) possess high specific strength, high specific modulus, and excellent properties both at ambient and elevated temperature [2–4]. In comparison to most other aluminum-rich intermetallic phases, Al_3Ti is very attractive because it has a higher melting point (~1350 °C) and relatively low density (~3.3 g/cm^3). Further, Ti has low diffusivity and solubility in aluminum [5], hence Al_3Ti can be expected to exhibit low coarsening rate at elevated temperature. By non-equilibrium processing technique like rapid solidification processing (RSP) and mechanical alloying (MA), Al–Al_3Ti composites with different volume fraction of Al_3Ti reinforcement can be developed. However, room temperature brittleness of Al_3Ti limits its industrial applications [6]. In the past two approaches have been attempted in order to improve the ductility of Al_3Ti, [7]. The first one was the micro alloying of DO_{22} structure but with little success [8]. The second approach, that is more popular, is to transform the DO_{22} structure to the $L1_2$ (ordered cubic) structure by the addition of a number of ternary elements [7–9]. The $L1_2$ structure has a higher symmetry so a larger number of slip systems and hence is expected to be have better ductility. The various elements that have been tried for this are Cr, Cu, Fe, Ni, Mn, Co, etc [10–13]. However single phase $L1_2$–Al_3Ti prepared by conventional casting route did not yield high ductility [9]. Grain refinement is a suggested viable method for making any intermetallics ductile [8]. Microstructural refinement to nanometer level is expected to increase both strength and ductility of intermetallics.

Attempts have been made earlier on formation of Al-based nanocomposites reinforced with $L1_2$–Al_3Ti particles in rapidly solidified binary Al–Ti alloys [14–16] and also with ternary addition into binary Al–Ti alloys [17–19]. In previous reports only three ternary elements such as Ce [18], Gd [17] and Ni [19] were attempted to achieve the stability of $L1_2$–Al_3Ti intermetallic dispersions in α-Al matrix. Nie and Muddle [19] have reported that the microstructure of rapidly solidified Al–Ti–Ni alloys, with a Ti:Ni weight ratio in the range of 3:1–4:1, invariably contained a uniform, fine-scale dispersion of cuboidal particles of a noble metastable fcc phase (space group Fm3c, $a = 2.42 \pm 0.01$ nm).

* Corresponding author: Center for Advanced materials Joining, University of Waterloo, Canada. Tel.: +1 519 888 4567x35256; fax: +1 519 888 6197.
E-mail addresses: sashank@uwaterloo.ca, sashank.nayak@gmail.com (S.S. Nayak).

0966-9795/$ – see front matter © 2009 Elsevier Ltd. All rights reserved.
doi:10.1016/j.intermet.2009.09.009

The present work is aimed at the synthesis of nanocomposites in Al–Ti alloys by RSP and study of their mechanical properties (hardness) at ambient as well as high temperatures. The present work also attempts to study the influence of Cr addition on the stabilization of $L1_2$–Al_3Ti phase in the nanocomposites formed by RSP, which was not studied so far.

2. Experimental details

Mother alloys with nominal compositions $Al_{100-x}Ti_x$ ($x = 4.1$, 5, 8.3, 10, 15 and 20[1]) and $Al_{100-4.1x}Ti_{3.1x}Cr_x$ ($x = 0.5$, 1.0 and 2.0) were prepared from high purity elements by arc melting under argon atmosphere and chill-casting on a water cooled copper hearth. The alloys were rapidly solidified, in an argon atmosphere, by melt spinning on to a rotating Cu wheel with wheel surface velocities of 30 m/s and 40 m/s. Depending upon the compositions and cooling rate (wheel surface velocity), melt spun ribbons were 1–4 mm wide and 15–50 μm thick. Phase analysis of melt spun ribbons was carried out by X-ray diffraction (XRD) with Cu-K_α radiation. The crystallite size of the as-spun nanocomposites was calculated from XRD peak profile using Scherrer formula after eliminating the instrumental and strain broadening [20]. The as-spun ternary Al–Ti–Cr alloys were annealed at different temperatures in a quartz tube under vacuum.

Microstructure of spun ribbons of Al–Ti alloys and Al–Cr–Ti alloys was examined in JEOL JEM 2000EX and PHILIPS CM20 transmission electron microscope (TEM), respectively. The samples for TEM observations were thinned for electron transparency by ion milling maintaining the specimen at −30 °C using liquid nitrogen. Microhardness measurements were carried out using a Vickers diamond indenter at a load of 10 g with a dwelling time of 15 s. Around 10–15 measurements were made on each sample to ensure the reproducibility of the hardness values. Nanoindentation on binary Al–Ti alloys melt spun at 40 m/s were carried for the measurement of hardness and elastic modulus by MTS Nano Indenter® XP using a diamond Berkovich indenter. For both micro and nano hardness measurements, all samples were mounted and mirror polished to flat surface.

3. Results and discussion

3.1. Nanocomposites in binary Al–Ti alloys

XRD patterns of the as-cast and melt spun (at 30 m/s) binary Al–Ti alloys (4.1Ti and 8.3Ti) are shown in Fig. 1a. In both as-cast alloys, equilibrium Al_3Ti (DO_{22}) and Al were observed. The volume fraction of DO_{22} phase in as-cast alloys is higher at higher Ti content in the alloy, as is evident by the higher DO_{22} peak intensity in Al-8.3Ti alloy in comparison to Al-4.1Ti alloy. In the melt spun alloys, along with the equilibrium phases, metastable $L1_2$–Al_3Ti also was observed (Fig. 1a). The volume fraction of $L1_2$–Al_3Ti phase in melt spun alloys is higher at higher Ti content. The peaks of $L1_2$–Al_3Ti phase are found as shoulder to Al peaks. However, superlattice reflections of $L1_2$–Al_3Ti, *viz.*, (100) and (110) were not found. The reason for the absence of superlattice reflection of $L1_2$–Al_3Ti phase forming in Al–Ti alloys is the small difference in the atomic scattering factors of Al and Ti as reported earlier [12,13,21]. These results indicate that rapidly solidified Al–Ti alloys form both equilibrium (DO_{22}) as well as metastable ($L1_2$) Al_3Ti intermetallic in α-Al matrix.

Fig. 1b shows the XRD patterns of $Al_{100-x}Ti_x$ for $x = 5$,10,15 and 20 alloys melt spun at 40 m/s. The figure indicates that higher cooling rate has resulted in complete suppression of DO_{22}–Al_3Ti phase in the alloys up to 15%Ti. The alloys with 5, 10 and 15%Ti showed a mixture of α-Al and $L1_2$–Al_3Ti intermetallic. The volume fraction of $L1_2$ phase increased with increase in Ti content in the alloy upto 15%. The Al-20Ti alloy melt spun at 40 m/s showed a large volume fraction of equilibrium DO_{22} structure of Al_3Ti along with some α-Al. Table 1 enlists the phases present, volume fraction of $L1_2$–Al_3Ti, the lattice parameter of $L1_2$ phase and the solubility of Ti in Al in all binary Al–Ti alloys melt spun at a linear wheel speed of 40 m/s. It is well known that non-equilibrium processing routes,

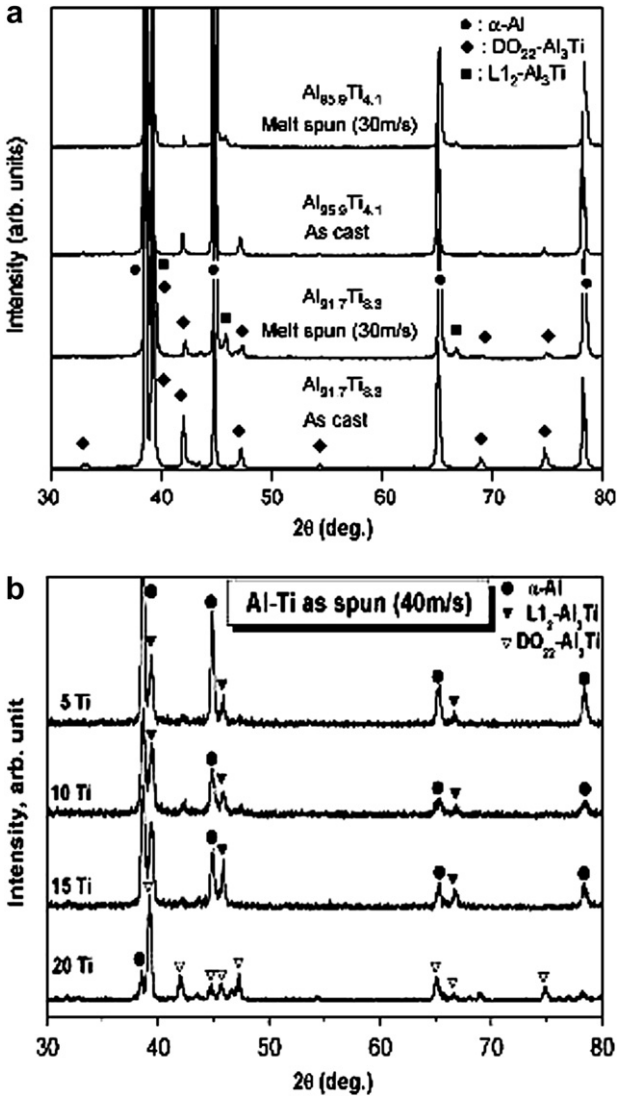

Fig. 1. XRD patterns of (a) as-cast and melt spun (30 m/s) Al-4.1Ti and Al-8.3Ti alloys and (b) $Al_{100-x}Ti_x$, $x = 5$, 10, 15 and 20, alloys melt spun at higher cooling rate (40 m/s).

Table 1
Comparison of microstructures, volume fraction of $L1_2$–Al_3Ti, the lattice parameter of $L1_2$-phase and the solubility of Ti in Al in all binary Al–Ti alloys, melt spun at a linear wheel velocity of 40 m/s.

Composition	Phases formed	Volume fraction of $L1_2$ phase	a-$L1_2$, nm	Ti solubility in α-Al, at.%
5 Ti	α-Al + $L1_2$–Al_3Ti	~24%	0.3960	1.4
10 Ti	α-Al + $L1_2$–Al_3Ti	~38%	0.3958	2.0
15 Ti	α-Al + $L1_2$–Al_3Ti	~42%	0.3961	2.8
20 Ti	α-Al + DO_{22}–Al_3Ti	~78% (DO_{22})	–	1.0

[1] All compositions are in atomic percent unless otherwise mentioned.

Please cite this article in press as: Nayak SS, et al., Microstructure-hardness relationship of Al–($L1_2$)Al..., Intermetallics (2009), doi:10.1016/j.intermet.2009.09.009

viz., RSP and MA, extend the solid solubility in any metallic system. In Al–Ti alloys, Ti is known to decrease the lattice parameter of Al being small in atomic radius compared to Al [12,13,21,22]. 1 at.% Ti decreases the lattice parameter of Al (0.405 nm) by 0.001 nm [22]. In the present work the solid solubility of Ti in Al was found from the change in lattice parameter of Al, which was calculated from the XRD results. The volume fraction of the different phases present in the alloys was calculated using the ratio of relative integrated intensities of the phase measured from the XRD profile using the following approach.

$$C_A = \frac{I_A}{I_A + I_B},\ C_B = \frac{I_B}{I_A + I_B}$$

where C_A and C_B are the volume fractions, I_A and I_B are the relative integrated intensities of the most intense peaks of A and B phases, respectively. An increase in volume fraction of $L1_2$–Al_3Ti phase from 24% to 42% is evident from Table 1 when the Ti content of the alloy is increased from 5% to 15%. Al-20Ti alloy has a high volume fraction (78%) of equilibrium DO_{22} phase instead of $L1_2$ phase observed in lower Ti containing alloys. The crystallite size of α-Al was found in the range of 20–30 nm, while that of $L1_2$–Al_3Ti phase was found to be in the range 20–25 nm indicating for formation of nanocomposites by RSP.

Fig. 2a and b shows the bright field images of Al-5Ti and 15Ti alloys, respectively, melt spun at a wheel surface velocity of 40 m/s. Formation of a two phase mixture containing $L1_2$–Al_3Ti intermetallic particles embedded in α-Al matrix was observed in both the cases. The $L1_2$–Al_3Ti particles were found to have more or less spherical morphology. Most of the particles were found in the size range 80–100 nm. However, few coarser particles in the size range 0.4–0.5 μm were also found. Insets of Fig. 2a and b are the selected area diffraction patterns (SADP) taken from the Al_3Ti particles confirming the $L1_2$ structure of Al_3Ti phase.

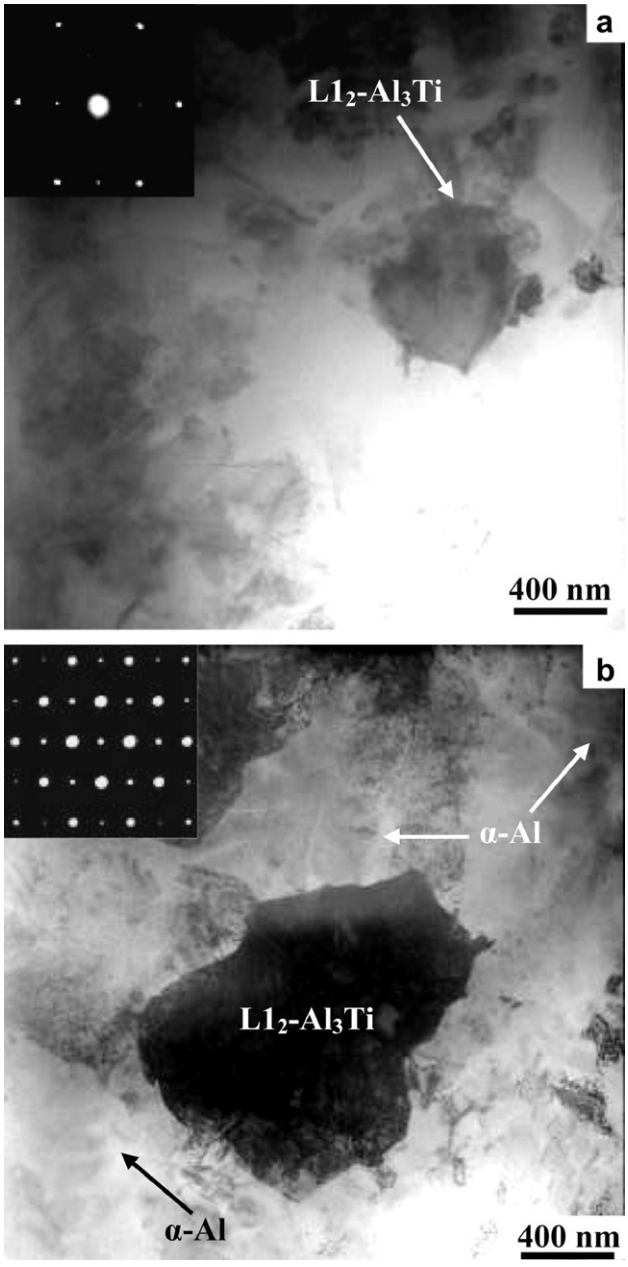

Fig. 2. Bright field images of (a) Al-5Ti and (b) Al-15Ti alloys melt spun at 40 m/s wheel velocity. Insets are the selected area diffraction patterns from the $L1_2$–Al_3Ti particles in respective alloys.

3.2. Nanocomposites with Cr addition to dilute Al–Ti alloy

Ternary addition of Cr into binary dilute Al–Ti alloys was made keeping the Ti:Cr ratio approximately 3.2:1 for stabilization of $L1_2$–Al_3Ti

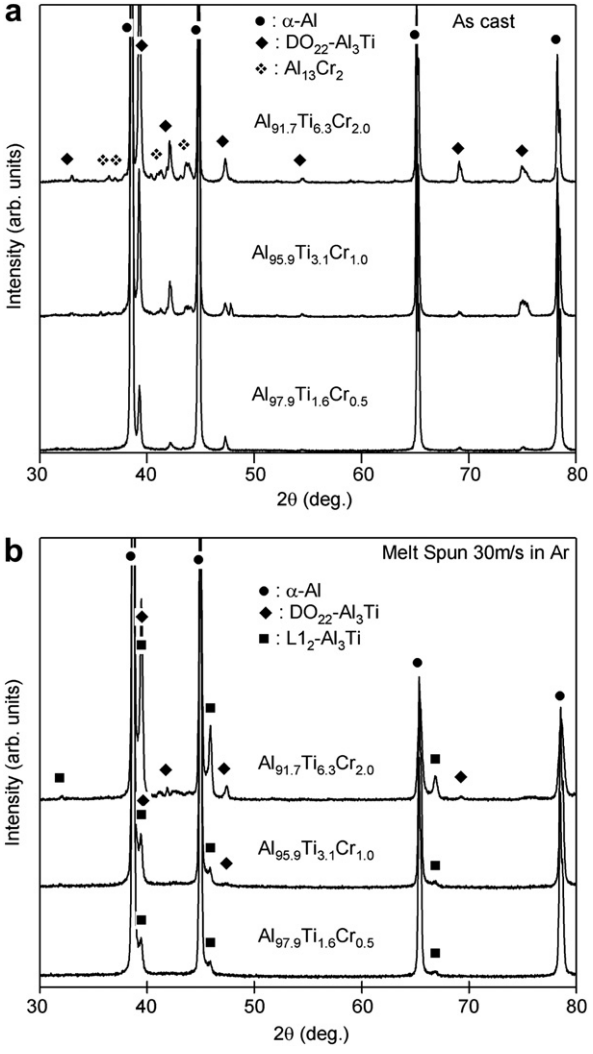

Fig. 3. XRD patterns of (a) as-cast and (b) melt spun (30 m/s) ternary Al-1.6Ti-0.5Cr, Al-3.2Ti-1.0Cr and Al-6.3Ti-2.0Cr alloys.

Please cite this article in press as: Nayak SS, et al., Microstructure-hardness relationship of Al–($L1_2$)Al..., Intermetallics (2009), doi:10.1016/j.intermet.2009.09.009

phase, based on the earlier studies on conventionally cast alloys [7,9]. Dilute Al–Ti–Cr alloys with three different compositions were chosen to prepare the nanocomposites of α-Al and $L1_2$–Al_3Ti with different volume fractions of $L1_2$–Al_3Ti. The XRD patterns of the as-cast and melt spun alloys at the wheel surface velocity of 30 m/s are shown in Fig. 3a and b, respectively. In as-cast alloys, formation of α-Al and DO_{22}–Al_3Ti along with Al_3Cr_2 was observed. Volume fraction of DO_{22}–Al_3Ti has increased with increase in the Ti content in the alloys as expected. However, in spite of the Cr additions, formation of equilibrium DO_{22}–Al_3Ti could not be suppressed in the as-cast alloys. Melt spinning of the as-cast alloys with a linear wheel surface velocity of 30 m/s resulted in the formation of $L1_2$–Al_3Ti along with α-Al with volume fraction of $L1_2$–Al_3Ti phase increasing with increasing Cr and Ti content in the alloys as shown in Fig. 3b. However, a small amount of equilibrium DO_{22}–Al_3Ti was found in higher solute containing alloy (Al-6.3Ti-2.0Cr).

In melt spun Al-1.6Ti-0.5Cr alloy, the microstructure was equi-axed with grain sizes in the range of 0.5–1 μm as shown in Fig. 4. Dispersion of fine-scale intermetallic particles in the size range of 40–50 nm in equiaxed α-Al grains as well as at the grain boundaries was observed in this alloy. The dispersed particles were confirmed to be $L1_2$–Al_3Ti phase from the SADP obtained from these particles. The inset in Fig. 4a shows the [011] zone axis of cubic phase with the presence of less intense superlattice diffraction spots indicating the ordered structure of $L1_2$–Al_3Ti.

The effect of increase in total solute content in the alloys resulted in obvious increment in the volume fraction of $L1_2$–Al_3Ti phase in microstructure of melt spun Al-3.2Ti-1Cr alloy (Fig. 4b). Dispersion of intermetallic particles was more uniform and they were mostly found inside the grains of α-Al in this alloy compared to low solute containing alloys. The SADP shown as inset in Fig. 4b confirmed their $L1_2$ ordered structure. Further increase in the total solute content in the alloy (Al-6.3Ti-2Cr) has resulted in an increase in size and volume fraction of intermetallic particles as shown in Fig. 4c. The $L1_2$–Al_3Ti particles were seen to be spherical with the size range of 50–80 nm.

The $L1_2$–Al_3Ti phase is expected to nucleate in the melt prior to the nucleation of α-Al and during further solidification they are trapped by the fast moving solid–liquid interface of α-Al phase [23]. Further the fine-scale distribution of the $L1_2$–Al_3Ti implies that their formation involves high rate of nucleation and slow rate of growth during rapid solidification. It is also possible that $L1_2$–Al_3Ti forms as a product of micro-cellular solidification, in which small pockets of solute-rich phase are pinched off behind fast moving cellular interface [24]. This is more prominent in Al-6.3Ti-2Cr alloy which forms the spheroidal intermetallic particles similar to the result of the micro-cellular solidification. The entrapment of liquid droplet behind a cellular interface requires a critical interface velocity and a critical level of undercooling in the melt. It is to be noted that there was no indication of any other phase formation in the nanocomposite apart from Al and $L1_2$–Al_3Ti phases.

3.3. Hardness of nanocomposites with $L1_2$–Al_3Ti precipitates

It may be mentioned here that evaluation of mechanical properties of the nanocomposites prepared in the present study was

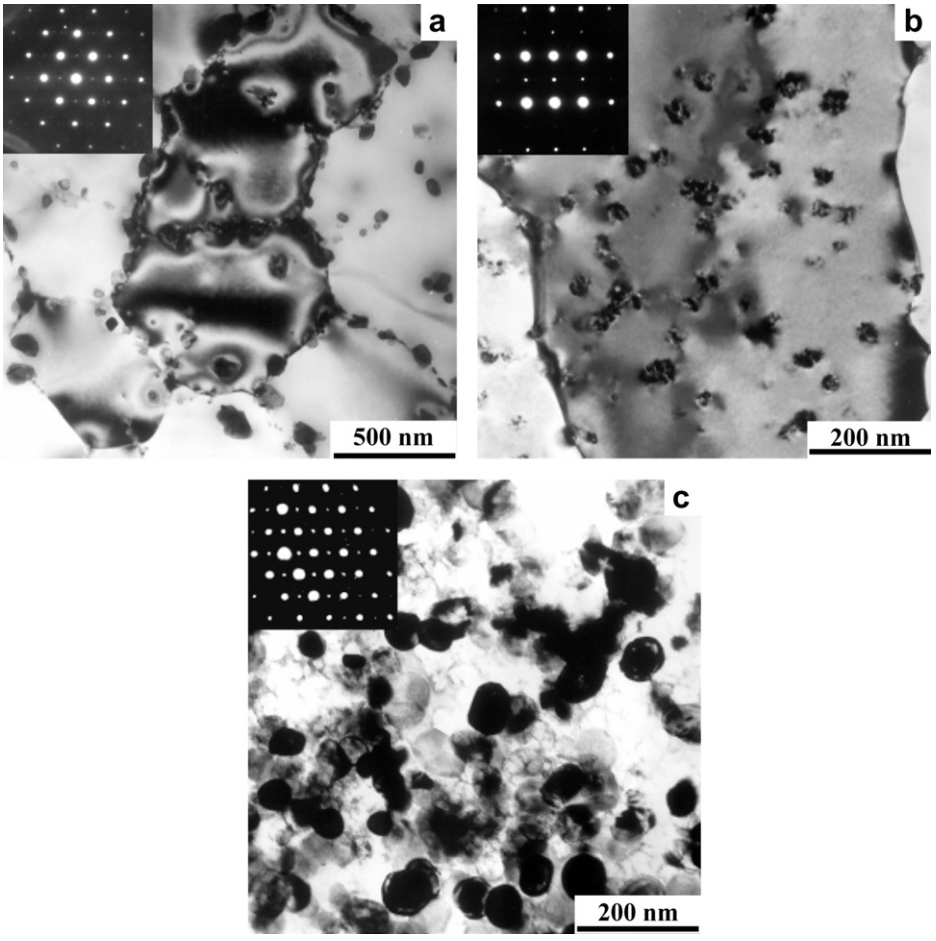

Fig. 4. Bright field TEM images of (a) Al-1.6Ti-0.5Cr, (b) Al-3.2Ti-1.0Cr and (c) Al-6.3Ti-2.0Cr alloys melt spun at 30 m/s. Insets are the SAD patterns of the $L1_2$–Al_3Ti particles.

Please cite this article in press as: Nayak SS, et al., Microstructure-hardness relationship of Al–($L1_2$)Al..., Intermetallics (2009), doi:10.1016/j.intermet.2009.09.009

beyond the scope of the work. However, detailed evaluation of hardness at room temperature as well as at high temperature has been carried out. In the present work hardness was evaluated as an indirect method to assess the strength of the nanocomposites. The variation of Vickers hardness of the nanocomposites that formed in rapidly solidified binary Al–Ti alloys is shown in Fig. 5a. The hardness increases with increase in Ti content in the alloy, which is a consequence of increased volume fraction of $L1_2$–Al_3Ti in the nanocomposites as shown in Table 1, indicating possibility of decrease in ductility. Hardness increases from 178 VHN (1.81 GPa) to 340 VHN (3.46 GPa) with an increase in Ti content in the alloy from 5 to 15, with an associated increase in volume fraction of $L1_2$–Al_3Ti from 24% to 42%. The hardness values of 20% Ti containing alloy could not be measured due to its brittle nature. This is attributed to the formation of high volume fraction of brittle DO_{22}–Al_3Ti phase. The high hardness of the nanocomposites in the present work is attributed to three main factors mainly (1) strengthening due to formation of $L1_2$–Al_3Ti intermetallic, (2) solute solution strengthening due to high solute content (1.4–2.8% Ti) in α-Al matrix, and (3) grain size refinement of both α-Al matrix and embedded intermetallic particles in the nanometer range.

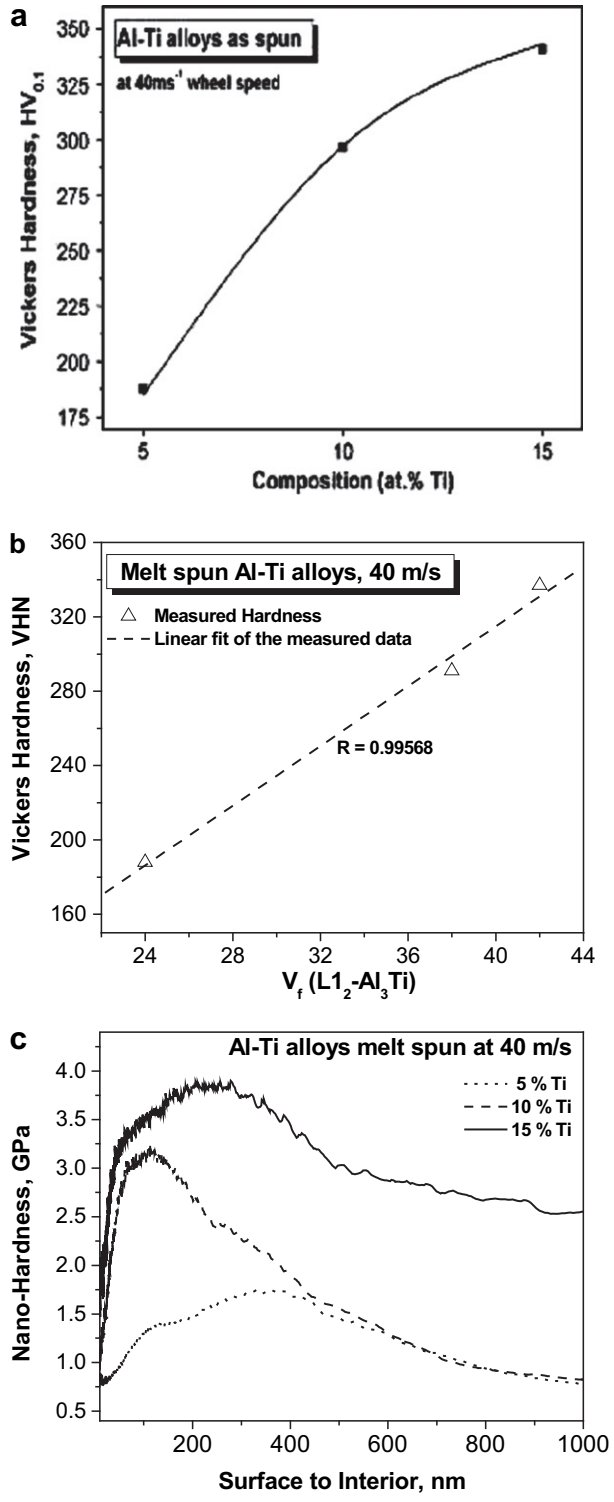

Fig. 5. Hardness of Al–Ti alloys melt spun at 40 m/s wheel velocity. (a) Variation of Vickers hardness with Ti content, (b) Variation of Vickers hardness with volume fraction of $L1_2$–Al_3Ti phase in the nanocomposites, and (c) Hardness variation in nanoindentation studies with depth from the surface.

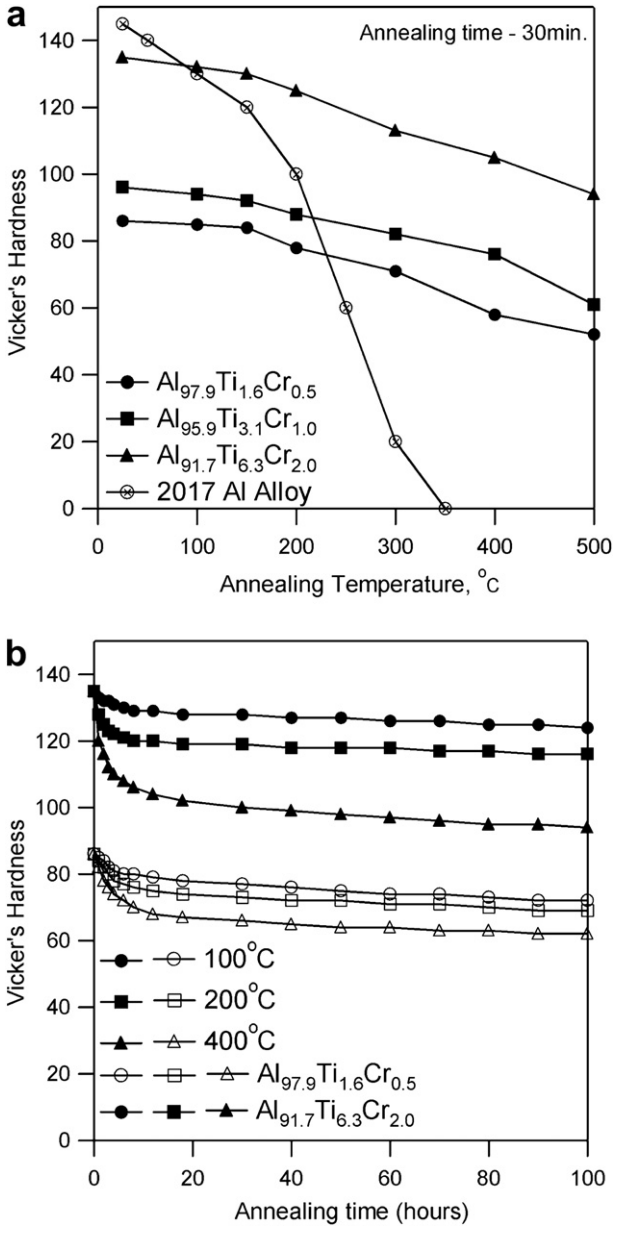

Fig. 6. Variation of Vickers hardness of melt spun ternary Al-1.6Ti-0.5Cr, Al-3.2Ti-1.0Cr and Al-6.3Ti-2.0Cr alloys with (a) temperature and comparison with conventional 2017 Al alloy, and (b) holding time at temperature 100, 200 and 400 °C.

Please cite this article in press as: Nayak SS, et al., Microstructure-hardness relationship of Al–($L1_2$)Al..., Intermetallics (2009), doi:10.1016/j.intermet.2009.09.009

The effect of volume fraction of $L1_2$–Al_3Ti on the hardness values of the nanocomposites follows a linear relationship (Fig. 5b) with a regression coefficient R^2 of 0.996. Nanoindentation studies were carried out to confirm the high hardness values of the nanocomposites. Variation of hardness (GPa) from the surface to interior of the nanocomposites is plotted in Fig. 5c. Hardness is high generally at the surface (up to 400 nm) of the nanocomposites and decreases towards the interior. As observed from Vickers hardness measurement (Fig. 5a), nanoindentation also gives high hardness value of 1.72 and 3.75 GPa (~168 VHN and 367 VHN) for the Al-5Ti 15Ti alloys, respectively. This confirms the high hardness of the Al–($L1_2$)Al_3Ti nanocomposites of binary Al–Ti alloys prepared by RSP.

In contrary to melt spun binary Al–Ti alloys, rapidly solidified ternary Al–Ti–Cr alloys have shown lower hardness values in the range 85–138 VHN (Fig. 6a), which could be attributed to lower solute content and lower wheel velocity (lower cooling rate) used (30 m/s). However, increase in hardness values (138 VHN) with increasing overall solute content, leading to an increase in volume fraction of $L1_2$–Al_3Ti phase, was observed. Hot hardness studies of the nanocomposites after holding the alloy for 30 min at different temperatures did not change the hardness values very much. The hardness value decreased from 138 VHN at room temperature to 100 VHN (aged at 500 °C) in case of high solute containing alloy. So the nanocomposite retained about 72% of its hardness even at high temperature of 500 °C. In contrast, conventional 2017 Al alloy showed a rapid fall in the hardness values from 142 VHN to almost close to 0 VHN after holding the alloy at 350 °C for 30 min. The sluggish decrease in hardness of the nanocomposites to high temperature exposure is attributed to the stability of the intermetallic particles, which has very low tendency to dissolve in the matrix due to the low solubility of Ti in Al. It has also been reported by the present authors that thermal stability of $L1_2$ phase of Al_3Ti intermetallic is best achieved with Cr as the ternary addition compared to other transition metals, *viz.*, Cu, Fe, Ni, Co and Mn [12].

Fig. 6b compares the hot hardness values melt spun Al-6.3Ti-2.0Cr and Al-1.6Ti-0.5Ti alloys exposed to 100, 200 and 400 °C up to 100 h. In both the alloys, nanocomposites lose their hardness faster at higher temperature 400 °C up to 20 h and the hardness remains more or less constant after that (Fig. 6b). However, the drop in hardness value is sharper in the alloy with higher solute content. At lower temperature of 100 and 200 °C, no significant drop in hardness was observed in both the nanocomposites up to 100 h. It can be concluded from these results that the nanocomposites with nanocrystalline $L1_2$–Al_3Ti intermetallic particles embedded in ultra-fine α-Al matrix can be used for high temperature applications.

4. Conclusions

1. Aluminum based nanocomposites with nanocrystalline $L1_2$–Al_3Ti precipitates have been successfully prepared in binary Al–Ti alloys as well as in ternary Al–Ti–Cr alloys by rapid solidification processing. Cr has been shown to be a stabilizer of $L1_2$ structure of Al_3Ti in the rapidly solidified alloys. Higher cooling rate has helped in the suppression of the equilibrium DO_{22}–Al_3Ti phase.
2. Hardness values of binary Al–Ti were observed to increase with increase in volume fraction of $L1_2$–Al_3Ti. High hardness of 340 VHN (~3.46 GPa) was measured for the nanocomposite with 42% volume fraction of $L1_2$–Al_3Ti in Al-15Ti alloy. Nanoindentation studies of the same alloy measured a similar hardness of 367 VHN (~3.75 GPa).
3. The nanocomposites formed in ternary Al–Ti–Cr alloys retain 70–85% of their room temperature hardness even at 500 °C for 100 h indicating the possibility of high temperature application of these alloys.
4. Low drop in hardness of nanocomposites is due to the stability of $L1_2$ phase at high temperature.

Acknowledgement

S.S. Nayak is thankful to Prof. D.H. Kim for providing support to carry out part of this work at Center for Noncrystalline Materials, Yonsei University; Seoul, South Korea. The authors acknowledge the help of H.J. Chang, a doctoral student at Yonsei University, for the electron microscopy studies.

References

[1] Ryum N. Acta Metall 1969;17:269.
[2] Tong XC, Fang HS. Metall Mater Trans A 1998;29A:893.
[3] Wang SH, Kao PW. Acta Mater 1998;46:2675.
[4] Varin RA. Metall Mater Trans A 2002;33A:193.
[5] Das SK, Davis LA. Mater Sci Eng A 1988;98:1.
[6] Pandey AB, Mishra RS, Mahajan YR. Acta Metall Mater 1992;40:2045.
[7] Yamaguchi M, Umakoshi Y. Prog Mater Sci 1990;34:1.
[8] Baker I, Monroe PR. J Met 1988;40:28.
[9] Yamaguchi M, Inui H. Al3Ti and its L12 variations. In: Westbrook JH, Fleischer RL, editors. Intermetallic compounds, vol. 2. New York: Wiley; 1994. p. 147.
[10] Mazdiyasni S, Miracle DB, Dimiduk DM, Mendiratta MG, Subramanian PR. Scr Metall 1989;23:327.
[11] Mabuchi H, Hirukawa K, Tsuda H, Nakayama Y. Scr Metall 1990a;24:505.
[12] Nayak SS, Murty BS. Mater Sci Eng A 2004;367:218.
[13] Nayak SS, Murty BS. Trans Indian Inst Met 2003;56:457.
[14] Majumdar A, Muddle BC. Mater Sci Eng A 1993;169:135.
[15] Hori S, Tai H, Narita Y. In: Steeb S, Warlimont H, editors. Rapidly quenched metals. Amsterdam: Elsevier; 1985. p. 911.
[16] Nayak SS, Kim DH, Pabi SK, Murty BS. Trans Indian Inst Met 2006;59(2):193.
[17] Mahajan YR, Kirchoff SD, Froes FH. Scr Metall 1986;20:643.
[18] Nie JF, Muddle BC. Metall Mater Trans A 1992;23:3193.
[19] Nie JF, Muddle BC. Mater Sci Eng A 1996;215:92.
[20] Klug HP, Alexander L. X-ray diffraction procedures for polycrystalline and amorphous materials. New York: Wiley; 1974. p. 661.
[21] Nayak SS, Pabi SK, Murty BS. Intermetallics 2007;15:26.
[22] Pearson WB. A hand book of lattice spacings and structures of metals and alloys. Oxford: Pergamon; 1974.
[23] Cotton JD, Kaufman MJ. Metall Mater Trans A 1991;22:927.
[24] Boettinger WJ, Bendersky LA, Schaefer RJ, Biancaniello FS. Metall Mater Trans A 1988;19:1101.

Please cite this article in press as: Nayak SS, et al., Microstructure-hardness relationship of Al–($L1_2$)Al..., Intermetallics (2009), doi:10.1016/j.intermet.2009.09.009